POLITECNICO DI TORINO
Repository ISTITUZIONALE

3D Printed Metallic Pillar Nanomechanical Resonators Decorated with TiO2 Nanotubes for Highly Sensitive Environmental Applications

(Article begins on next page)

12 May 2025

3D Printed Metallic Pillar Nanomechanical Resonators Decorated with TiO$_2$ Nanotubes for Highly Sensitive Environmental Applications

*Andrea Lamberti, Marco Laurenti, Diego Manfredi, Carlo Ricciardi, and Stefano Stassi**

Micro and nanomechanical devices offer enhanced sensing capabilities for detecting biological and chemical small molecules. However, miniaturization necessitates advanced fabrication processes and complex measurement systems, hindering routine sensor analysis. While alternative methods like 3D printing show promise, challenges such as low device resolution persist due to intrinsic damping of polymer inks. In this study, an array of micrometric pillar resonators is fabricated in Ti6Al4 V alloy using additive manufacturing based on laser powder bed fusion technology. These metallic nanomechanical resonators exhibit a very high quality factor with minimal difference between air and vacuum measurements due to low intrinsic damping. Furthermore, titania nanotubes grown on the pillars via anodic oxidation heighten sensitivity for molecular dye degradation evaluation. Leveraging the weak coupling phenomenon among the pillars in the array, these devices facilitate large-scale parallelized measurements, here demonstrated with real-time analysis of dye degradation process. This approach to creating mass sensing devices via metallic additive manufacturing can usher in a new generation of highly performing resonating sensor arrays, offering a cost-effective and efficient alternative to traditional silicon microfabrication methods.

1. Introduction

Micro and nanomechanical devices have been widely implemented as chemical and biological sensing for their performances in mass and force detection.[1–3] Research in resonators field has always aimed to provide improvements in terms of sensitivity and throughput. The reduction of standard silicon-based device dimensions in the nanoscale range and the implementation of 1D or 2D nanostructures (such as carbon

nanotubes or graphene membranes) have brought to a huge boost in resonator sensitivity.[4–6] On the other hand, these devices require complex measurement systems and advanced fabrication processes. Moreover, the reduced capture cross-section of these devices decreases the sensor throughput resulting not suitable for routine sensor analysis required in biological and chemical fields, but more target to fundamental studies. Instead, resonators in the MEMS range provide a good compromise between sensitivity and throughput performances, thanks to the possibility of fabricating arrays to parallelize the measurements and speed up the analysis.[7–10] We recently demonstrate an innovative approach to parallelize the measurement of up to 44 cantilever resonators exploiting weak-coupling phenomenon among the devices.[11]

Although the clear advantages of using Micro-ElectroMechanical Systems (MEMS) devices and arrays for sensing applications, as described above, a disadvantage is still represented by the complex and time-consuming fabrication process. Alternative fabrication methods to the silicon based processes have been widely investigated to speed up the fabrication and test new geometries and materials.[12] Screen printing,[13] hot embossing,[14] microinjection molding,[15] microfluidic approach[16] and 3D printing[17–20] are among the mostly investigated approaches. Among these techniques, 3D printing technologies represent the most flexible approach for the easiness of implementation and the possibility of adding intrinsic functionalities to the final device by tuning the composition of precursors materials. Digital light processing,[17,18] direct laser writing,[19,21] and stereolithography technique[20,22] have been investigated to fabricate MEMS resonators. Despite the possibility of introducing new functionalities directly inside the structural material, quality factor and thus device resolution remain low because of the intrinsic damping of the polymer ink used. Two photon polymerization has been used to overcome damping limitation of polymeric material by printing nanomechanical resonators with a metal-organic precursor solution, followed by a thermal step to remove organic content, finally obtaining a rigid inorganic resonating devices.[23] This last approach allows to reach the performances of

A. Lamberti, M. Laurenti, D. Manfredi, C. Ricciardi, S. Stassi
Department of Applied Science and Technology
Politecnico di Torino
Corso Duca Degli Abruzzi, 24, Torino 10129, Italy
E-mail: stefano.stassi@polito.it

**ADVANCED
SCIENCE NEWS**

www.advancedsciencenews.com

**ADVANCED
MATERIALS
TECHNOLOGIES**

www.advmattechnol.de
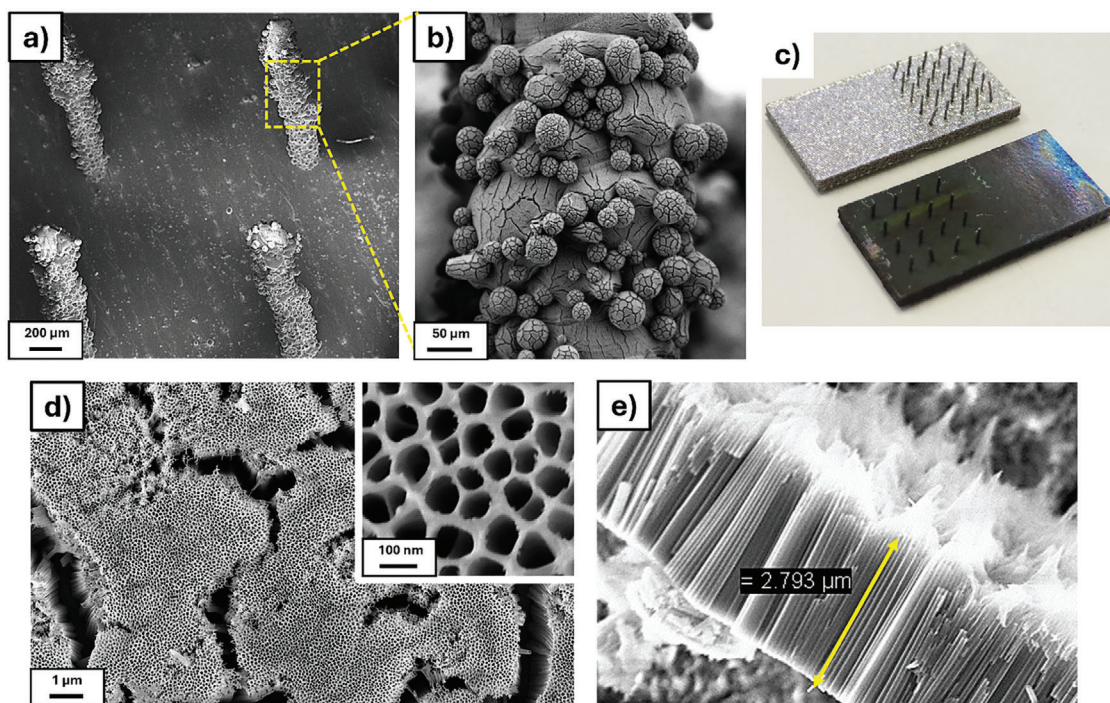
Figure 1. a,b) Field emission scanning electron microscopy (FESEM) images of the metallic printed pillars. c) Images of 3D printed metallic resoantors array before (above) and after (below) the titania natotubes grown. d,e) FESEM images of the annealed titania nanotubes grown onto the 3D printed Ti6Al4 V samples.

silicon-based devices, but is limited to the production of very small Nano-ElectroMechanical Systems (NEMS) device and needs a thermal step at high temperature.

In this work, we propose a solution to overcome complex fabrication approach of silicon based nanomechanical resonators. Herein, an array of micrometric pillars have been fabricated in a Ti6Al4 V alloy by additive manufacturing approach based on laser powder bed fusion (LPBF) technology, well know approach for the fast fabrication of structural prototypes and components.[24] The metallic resonators show a very high quality factor with low difference between air and vacuum measurement. Each resonator of the array resulted weakly coupled with the other resonators allowing the implementation of the whole device for large-scale parallelization measurements. In order to implement multifunctionality in this array, 1D titania nanotubes (NTs) have been grown on the pillar by anodic oxidation allowing an elevate sensitivity and parallelization measurement on the resonator surface and implementing the device for molecular dye degradation evaluation. Indeed, anodic oxidation is a process used to create 1D titanium dioxide (TiO_2) nanotubes, boasting a unique structure characterized by high surface area, which is crucial for catalytic reactions. What is really fascinating is that is possible to precisely tailor NTs properties during fabrication, adjusting factors like crystallinity and porosity to optimize their performance for specific reactions.[25,26] TiO_2 nanotubes properties position them as promising candidates for a wide range of applications, from environmental remediation to renewable energy production.[27–29] The 3D printed resonators decorated with titania NTs have been used to monitor dye degradation in real-time by using both main resonance peaks and weak coupling
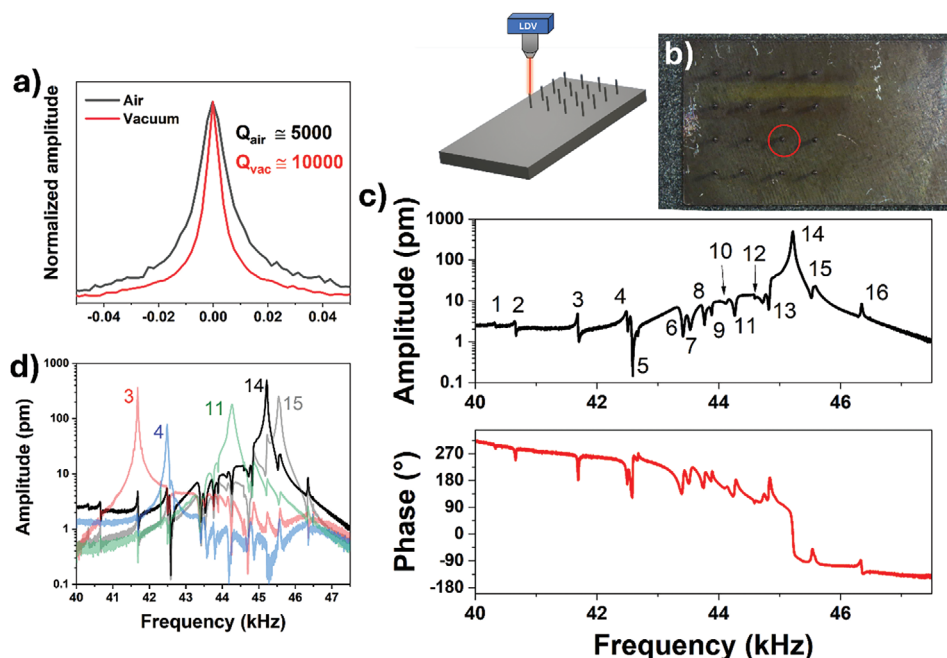
ones. The approach outlined for creating mass sensing devices via metallic additive manufacturing could pave the way for a new generation of highly performing resonating sensor arrays, circumventing the need for complex, time-consuming, and costly standard silicon microfabrication methods.

2. Results

Laser powder bed fusion (LPBF) technology enables the printing of metallic objects with intricate 3D shapes at a resolution in the micrometer range. This technology presents an intriguing opportunity for the rapid and straightforward fabrication of mechanical resonators. The materials compatible with this approach possess high mechanical stiffness, a crucial property for achieving mechanical resonators with a high quality factor, thereby enhancing sensor sensitivity.

The 3D samples produced through the LPBF method consist of a parallelepiped base measuring 10 mm x 20 mm x 1.2 mm (width, length, and thickness) for easy handling, topped with a 4×4 matrix of pillars measuring 200 μm in diameter and 1.5 mm in height. This configuration is illustrated and depicted in **Figure 1**a–c. The pillars comprise a core of molten and recrystallized Ti6Al4 V powder, with some metallic microparticles on the outer surface remaining partially fused by the laser scan. This variability in the final shape of each pillar is crucial for producing devices with slightly varying resonance frequencies, allowing for the exploitation of weak coupling among mechanical resonators, as described later.

The electrochemical growth of titania nanotubes proceeded through a three-step process. Initially, a ten-minute anodization

**ADVANCED
SCIENCE NEWS**

www.advancedsciencenews.com

**ADVANCED
MATERIALS
TECHNOLOGIES**

www.advmattechnol.de

Figure 2. a) Amplitude spectra of pillar resonator centered around the resonance mode measured in air (black) and vacuum (red) environment. *Q* values are extracted from Lorentzian fitting of the peaks. b) Scheme of the measurement set-up of the 3D printed metallic pillar resonator and image of the array with underlined by red circle the pillar analyzed in next spectrum. c) Vibration spectrum (black) and phase signal (red) of a pillar resonator of the array. The resonance peak of the pillar is the number 14. The other numbers count the weak-coupling peaks related to all the other 15 pillar resonators of the array. The numeration is related to the frequency position of the peaks (from lower to higher values) and not to their physical position in the array. d) Vibration spectra of 5 pillar resonators of the printed array to underline the relation of weak-coupling peaks with the other device resonance peaks. The spectrum shown in c) is represented with a black line, while all the others by coloured lines. The number of the pillars, using the same numeration of figure c), are reported close to each spectrum.

created a sacrificial layer of NTs. Subsequently, the disordered layer was eliminated via sonication in an hydrogen peroxide (H_2O_2) solution, resulting in a Ti6Al4 V surface marked by nearly periodic hollows formerly occupied by the removed NTs bottom, as documented in our prior research.[30] This textured surface promoted a more uniform distribution of debris-free NTs during the second anodization step. Following the removal of the second batch of NTs and a third round of growth, the morphology depicted in Figure 1d,e was achieved.

This refined procedure facilitated the creation of an organized array of nanotubes, ≈2.8 µm thick, firmly adhered to the Ti6Al4 V surface. The utilization of an organic solvent and high potential resulted in NTs with sleek walls, well-defined profiles, and rapid growth rates.

After the growth process, the functional substrates were characterized under dynamic actuation. When actuated by a piezodisk, metallic resonators are put in vibration with a frequency following the actuation signal one. Out of plane vibration of the metallic pillars is registered by a Laser Doppler Vibrometer (LDV) able to evaluate sub-picometer oscillations (scheme in **Figure 2**). The main resonance modes analyzed in these studies are predominantly characterized by in-plane motion due to the pillar geometries and boundaries. However, these vibrations also induce smaller out-of-plane movements, which can be easily detected by the LDV system. Vibrational spectra of the 3D printed metallic pillars are recorded both in air and vacuum to evaluate their mechanical and sensing properties (Figure 2a). The res-

onators show a resonance frequency peak with a quality factor *Q* of 10 000 in vacuum condition comparable with device fabricated with MEMS based technology.[23] Metallic additive manufacturing technology allows to reach high quality factor devices since these resonators are not limited by an elevate intrinsic damping. On the contrary, this limiting effect is dominating in 3D printed resonators fabricated with polymeric materials which could reach *Q* factors of the order of tens or hundreds. Moreover, when vibrate in air the printed metallic pillar resonators shows a very low viscous damping because of their shape, dimensions, and high material density. Quality factor is reduced only of a factor of two moving from vacuum to air environment, with a *Q* at ambient pressure of 5 000. This high quality factor guarantees a thin frequency lineshape for the resonance peak, with the possibility of detecting small frequency variations and thus having an elevate sensitivity. Therefore all the following measurements presented in this work have been conducted at ambient pressure.

Since the printed device is composed by an array of high quality factor resonators connected by a stiff substrate, a weak coupling phenomenon arise between the pillars, as evidenced by the presence of 16 peaks in the vibration amplitude and phase spectrum of Figure 2c (pillar resonator under analysis underlined in Figure 2b). Elastic coupling occurs in arrays of nanomechanical resonators when similar resonators are physically linked, causing their vibration response to be influenced by neighboring resonators. When the resonators are connected by an elastic support (normally a very thin one), a strong elastically

**ADVANCED
SCIENCE NEWS**

www.advancedsciencenews.com

**ADVANCED
MATERIALS
TECHNOLOGIES**

www.advmattechnol.de

coupling phenomenon give rise to collective modes of vibration, with non-localized eigenstates, that differ significantly from isolated resonators[31,32] Instead, when the resonators are connect by a rigid support (normally the bulk), like the metallic parallelepiped base of the printed device, the coupling among the resonators is small. In previous works of our group, we experimentally demonstrated and theoretically described that weak elastic coupling give rise to collective eigenmodes without delocalization of the eigenstate, like in strong coupling regime. The resonators in weakly coupling regime typically show collective eigenmode composed by a main Lorentzian vibrational response resembling that of a single resonator, along with additional peaks in the frequency spectrum corresponding to the eigenfrequencies of the other weakly connected resonators of the array, if considered individually.[11,33] These coupling peaks are usually significantly smaller in amplitude compared to the main resonance peak, making their detection challenging, but clearly evident in device with a high quality factors, since the coupling peak amplitude is proportional to resonator Q. In Figure 2c a vibration spectrum of a pillar (numbered as 14) is registered with the LDV system. Together with the main resonance peak of the pillar under investigation, other 15 low amplitude peaks appear both in the vibration amplitude and phase signal (numbered according to their frequency position in the spectrum). Each peak corresponds to another pillar resonator of the array and its amplitude is proportional to the related pillar Q factor and physical distance with respect of the resonator under investigation.[11] The slight physical differences and imperfections between each pillar, as clearly shown in Figure 1a, are crucial for creating pillar resonators with slightly varying resonance frequencies. As a result, the weak coupling peaks do not overlap in the vibrational spectrum of a single device, allowing them to be used for mass sensing analysis, as demonstrated later. The nature of the weak coupling peaks is clearly shown in Figure 2d overlapping to the amplitude spectrum already shown in Figure 2c with the spectra of other 4 pillars (not all the 16 spectra are shown together to avoid an unclear image). The weak coupling peaks are perfectly aligned with the Lorentzian peaks of the 5 resonators investigated. The presence of weakly coupling peaks for all the resonators of the array represents a powerful characteristic for the application of the printed device in sensing applications. As previously demonstrated, the use of weakly coupling peaks can parallelize the measurement of a whole sensor array, since each peak follow the variation of the resonance frequency of the corresponding resonator.[11,33] Therefore, measuring the vibration spectrum of a single resonator, it is possible to directly evaluate the frequency fingerprint of all the other resonators and thus of the whole device.

A crucial parameter for nanomechanical resonators, intended for use as biological or chemical sensors, is the active surface area. This area represents the available surface for binding the analyte during sensor detection. An easy and effective method to enhance the binding capability of resonators is by growing nanostructures on the device surface, as previously demonstrated by our group with zinc oxide nanowires or mesoporous silica film[34,35] The grown titania nanostructures on the printed metallic devices are composed of tiny, densely packed tubes, providing ample space for molecules to interact and react (Figure 1d,e).

The presence of nanotubes on the device surface does not significantly alter the resonator properties, as demonstrated in

Figure 3a. Examination of the resonance peak both before and after nanotube deposition reveals a decrease in resonance frequency due to the additional mass of oxygen, accompanied by a significant reduction in the Q factor to one-third of its initial value, from 4600 to 1640. However, this decline in property is rectified following the thermal curing process, during which residual synthesis materials are eliminated, and the titania NTs crystallize, thereby enhancing their structural rigidity. Consequently, both the resonance frequency and Q factor (3750) revert to values close to their initial levels, signifying the restoration of the device's functionality for sensing applications. Figure 3b illustrates that the resonators exhibit remarkably high quality factors for the first four resonance modes, even under ambient pressure conditions. The frequency stability of these modes was evaluated using Allan deviation analysis, revealing a theoretical sensor resolution below 10 ppb (parts per billion) for the first and second resonance modes and 100 ppb for the last two modes investigated. Since the resonance frequency f of a resonator can be expressed through its mass m and spring constant k as:
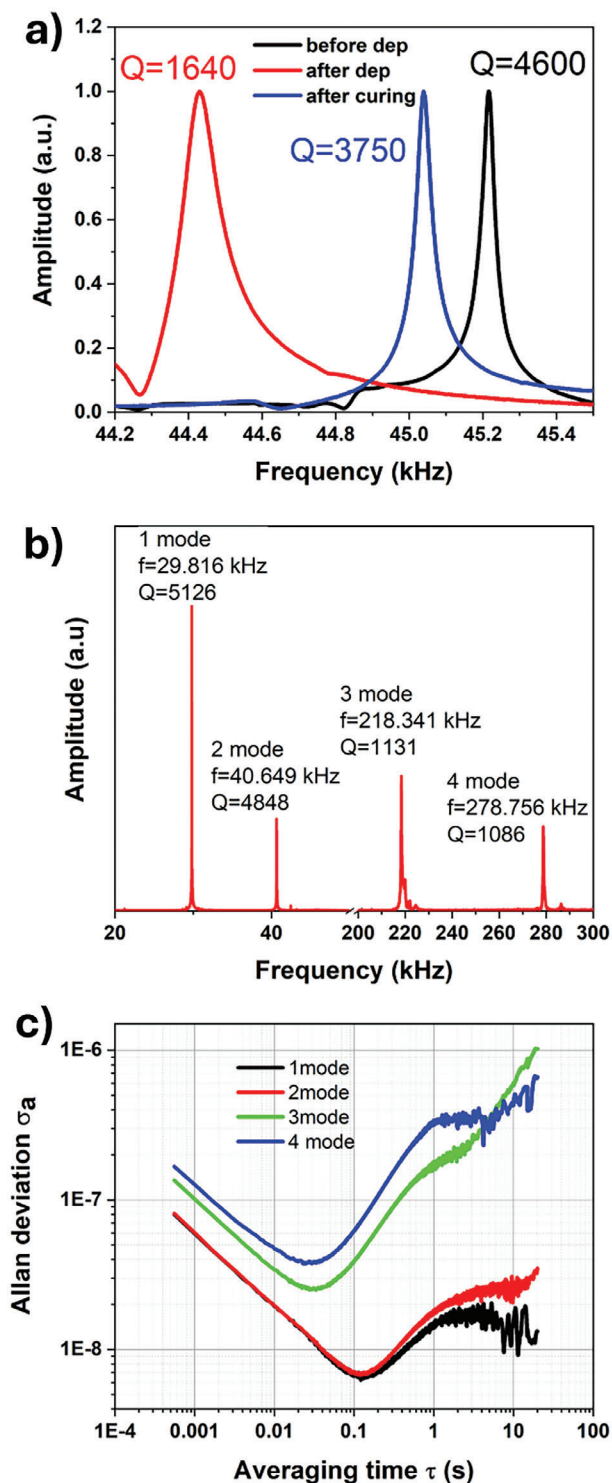
$$f = \frac{1}{2\pi} \sqrt{\frac{k}{m}} \tag{1}$$

small mass variation of the device can be directly related to a change in the measured frequency as follows:

$$\Delta m = -2m \frac{\Delta f}{f} \tag{2}$$

Therefore, given that the mass of the resonator is estimated to be 280 µg, the theoretical mass sensitivity of the 3D printed pillar falls within the picogram range, with a minimum sensitivity of 3.4 pg for the first two resonance modes. Measurements of Figure 3b,c were performed on pillar resonators after nanotube growth and annealing.
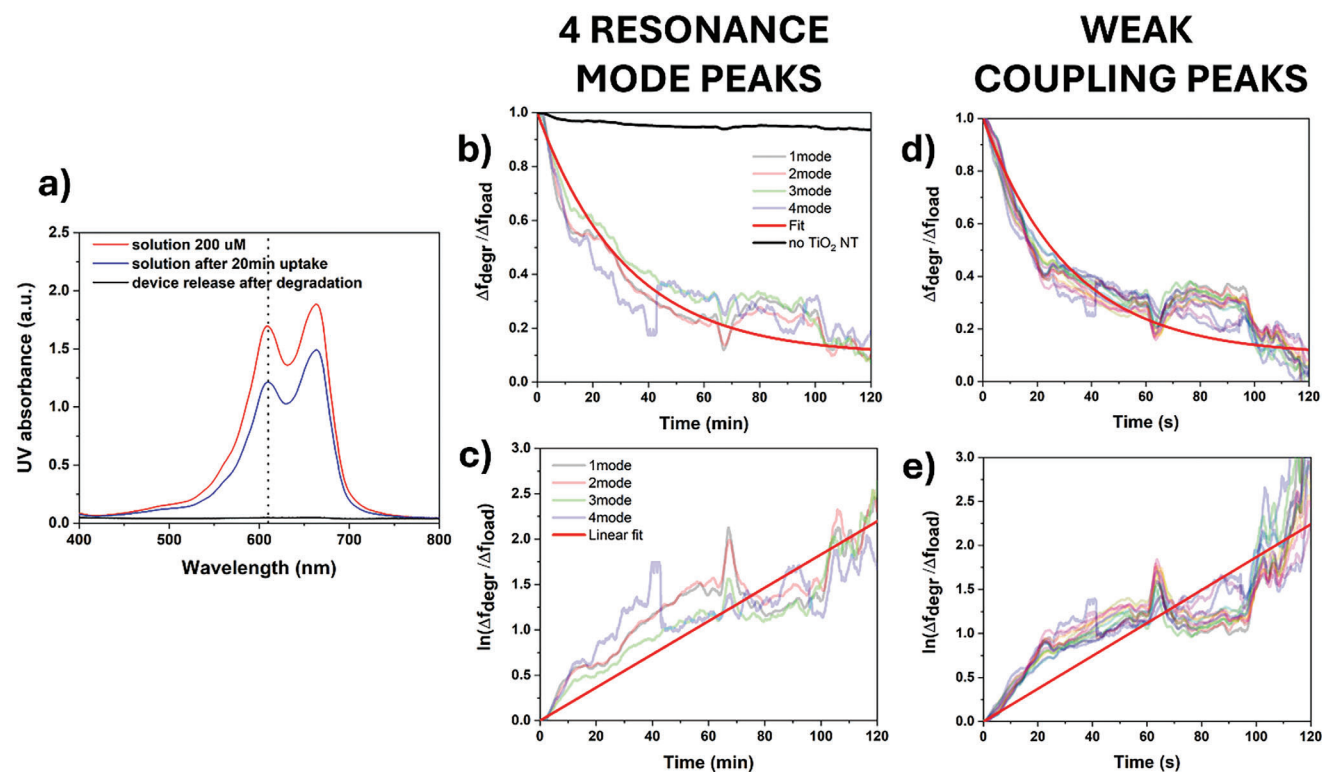
Furthermore, we showcase the sensor capabilities of the nanotube-decorated 3D printed metallic resonators, highlighting the facilitated parallelization measurement enabled by weak-coupling phenomena. The device demonstrates high sensitivity, utilized to monitor in real-time the degradation of an organic dye under UV illumination. In recent years, the issue of wastewater treatment has garnered significant attention due to the alarming depletion of clean water resources. Industrial dyes, in particular, contribute significantly to water pollution, rendering it unsuitable for drinking. Among these pollutants, methylene blue (MB) is particularly concerning due to its toxicity, carcinogenicity, and non-biodegradability, posing a severe threat to human health.[36] Therefore, monitoring the degradation process of this dye is crucial for assessing water pollution levels. The presented resonators could provide a viable solution for this purpose, given the well-known photocatalytic decomposition of various organic molecules on the titania surface, well documented and analyzed in the literature.[37–39] When TiO$_2$ is irradiated by photons with energies exceeding its band gap (in the UV range), electrons are excited from the valence band to the conduction band, leading to the formation of charge-carrier pairs. These generated free carriers can then react with dye and water molecules adsorbed on the outermost surface. Two processes occur: firstly, the photoinduced holes oxidize methylene blue molecules to methylene blue

**ADVANCED
SCIENCE NEWS**

www.advancedsciencenews.com

**ADVANCED
MATERIALS
TECHNOLOGIES**

www.advmattechnol.de

Figure 3. a) Evolution of the second mode resonance peak of a 3D printed metallic resonator before the deposition of titania nanotubes on the surface, after the deposition, and following thermal curing to crystallize the NTs. Q factor are reported close to each resonance peak. b) Amplitude vibration spectrum of the resonator displaying the first four resonance modes utilized for subsequent analyses. Frequency and Q factor values are provided adjacent to each resonance peak. A break in the frequency axis from 50 to 200 kHz is included to present all peaks in a single graph. c) Open-loop Allan deviation of the four resonance peaks depicted in b).

radicals ($\bullet$MB+), causing direct dye decoloration and degradation. Secondly, the reaction between the catalyst and the organic dye is mediated by highly reactive oxygen species (ROS) generated from the interaction of free electrons with the hydroxyl groups present in the chemical environment of the dye molecules. ROS can readily attack the dye molecule and induce its degradation. The photocatalytic activity of TiO_2 is influenced by its crystal structure, as defects serve as electron-hole recombination sites, thereby decreasing efficiency, and by surface area, which governs the contact between dye molecules and photocatalytic active sites. Titania nanotubes are optimal candidates for their anatase crystal structures and large active area[30]

In the degradation experiment, a device array consisting of 16 resonators was immersed for 20 min in a water-based solution containing 200 μм of Methylene Blue. Following a standard calibration procedure, the total amount of absorbed dye on the entire device was determined by calculating the difference between the UV–vis absorption curve values at 610 nm of the initial solution and after immersion of the sample (see **Figure** 4a). Evaluation of the active surface area of the device, comprised of the array base and pillars, revealed that a single resonator absorbed ≈480 ng of dye molecules. This absorbed mass value was further validated by the negative frequency shift observed in the first four resonance modes before and after dye absorption. Figure 4b illustrates the photocatalytic degradation of methylene blue molecules adsorbed on a single nanotube pillar resonator exposed to UV light. The degradation of MB is evident through the analysis of the frequency shifts in the four resonance modes, which increase with the conversion of the dye molecule into volatile species. The graph depicts the frequency shift of the four resonance modes (Δf_{degr}) normalized with respect to the shift observed during the loading of MB on the 3D printed pillars (Δf_{load}). Since UV illumination, along with dye degradation, causes heating of the resonator, affecting the resonance frequency value, a calibration of the resonator under illumination before MB loading was performed to eliminate this effect from the final measurement. All resonance modes confirm ≈90% degradation of the organic molecules after 2 h of illumination, with a remaining dye mass of 48 ng. A control experiment was conducted using a pillar without titania NTs loaded with MB, which exhibited minimal dye degradation (≈5%) due to UV-induced direct photolysis of methylene blue, confirming the dominant effect of the photocatalytic properties of TiO_2 nanostructures. The dye degradation on NT-decorated pillar resonator was also verified by immersing the sample in water after UV illumination to remove the remaining dye from the array. The UV–vis absorption curve of this solution indicated an 88% dye degradation, corresponding to a non-degraded mass per pillar of 55 ng, consistent with the data obtained from the resonance frequency measurements. The proposed technique offers a clear advantage over the standard method for evaluating dye degradation, which relies on punctual analysis of water solution at fixed time points. Continuous monitoring of the resonance frequencies enables real-time assessment of dye degradation, allowing observation of the complete process kinetics, which follows an exponential decay pattern, as expected from similar experiments.[40] Figure 4c reported the logarithms of the normalized frequency variation during the photodegradation of methylene blue. The data can be approximated with a

ADVANCED
SCIENCE NEWS

www.advancedsciencenews.com

ADVANCED
MATERIALS
TECHNOLOGIES

www.advmattechnol.de

Figure 4. a) UV absorption spectra of 200 μM Methylene Blue solution before and after dye absorption on 3D printed array, and of the solution prepared after the degradation experiment. The dashed line at 610 nm highlights the absorption peaks used for the quantification. b) Photocatalytic degradation of Methylene Blue absorbed on the surface of a 3D printed resonator, measured via a normalized resonance frequency shift related to the first four resonance modes. The red curve illustrates the exponential decay fit of the previous curves. The black curve represents the degradation of MB measured on pillar resonator without titania nanotubes. c) Logarithm of normalized pillar resonance shift shown in b). The red curve depicts the linear decay fit of the previous curves with a slope of 0.0186 min^{-1}. d) Photocatalytic degradation of Methylene Blue absorbed on the surface of all the 3D printed resonators of the array measured via the normalized resonance frequency shift of the 15 weak coupling peaks present in the vibration spectrum of the resonators analyzed in Figure b). The red curve illustrates the exponential decay fit of the previous curves. e) Logarithm of the normalized weak coupling frequency shift shown in d). The red curve represents the linear decay fit of the previous curves with a slope of 0.0186 min^{-1}.

linear trend, with some deviation for longer irradiation times due to measurement noise, indicating that the process can be described by pseudo first-order kinetics, as follows:

$$\ln\left(\frac{\Delta f_{degr}}{\Delta f_{load}}\right) = kt \qquad (3)$$

with k representing the kinetic rate constant defined as

$$k = \frac{\ln\left(\frac{\Delta f_{degr}}{\Delta f_{load}}\right)}{t} \qquad (4)$$

and computed as 0.0186 min^{-1}, value in line with other studies on dye photodegradation mediated by titania or other metal oxide nanostructures.[40–42]

As previously demonstrated, utilizing weak coupling peaks enables the assessment of the resonance modes of all resonators within an array by measuring the vibration spectrum of a single device. During the degradation experiments depicted in Figure 4b,c, the entire frequency response of a pillar resonator was continuously monitored over time. While the graph in question presents only the four resonance modes of the de-

vice, the same measurement encapsulates information regarding the degradation process occurring across all other resonators within the array. In Figure 4d,e, the temporal evolution of the weak coupling peaks associated with the other 15 pillars of the array is depicted (specifically for the first resonance mode). As anticipated, the trend and kinetic coefficient mirror those observed previously for the resonance frequency peaks, albeit with slightly more scattering due to the lower signal-to-noise ratio of the weak coupling peaks. Comparing the two methods, the use of higher-order resonance modes and weak coupling peaks, reveals both advantages and limitations for each approach. Higher-order resonance modes enable easier measurements because the vibrational amplitude of these modes is significantly greater than that of the weak coupling peaks, as clearly shown in Figure 2c,d. However, the higher-order resonance method can only monitor the evolution of a single resonator within an array, whereas the weak coupling approach can detect variations across all the pillars of the array. This broader detection capability allows for parallelized measurements of the entire array, which could be used to validate experimental results by analyzing multiple pillar sensors simultaneously. Additionally, it enables the monitoring of different experiments concurrently by functionalizing each pillar separately.

**ADVANCED
SCIENCE NEWS**

www.advancedsciencenews.com

**ADVANCED
MATERIALS
TECHNOLOGIES**

www.advmattechnol.de

The proposed approach offers clear advantages over standard contaminant degradation analysis methods, such as UV–vis measurements of solutions containing catalytic nanoparticles or nanostructured films, which are typically taken at different time points during the reaction.[39,41,43,44] The use of mechanical resonators allows for real-time monitoring of the degradation process. As demonstrated in this work and in previous research by Joo et al. on functionalized silicon cantilevers,[40] this approach also provides the potential for scaling up device arrays through 3D printing technology or microfabrication techniques. Additionally, the use of weak coupling phenomena paves the way for unprecedented measurement parallelization, which is not achievable with traditional degradation analysis methods.

3. Conclusion

In exploring the potential of laser powder bed fusion (LPBF) technology for fabricating mechanical resonators, our study foreseen promising results. We discovered that the 3D printed metallic resonators exhibited resonance frequencies and quality factors comparable to those produced using traditional MEMS-based techniques. This characteristic is crucial for ensuring sensor sensitivity. A notable finding was the occurrence of weak coupling among resonators within the device array. This phenomenon allowed for the parallelization of measurements, enabling the simultaneous assessment of multiple resonators. Through experimental measurements, we demonstrated that this weak coupling phenomenon facilitated continuous parallel monitoring of resonance frequencies from different resonators of an array. One significant improvement to our resonators was the functionalization with titanium dioxide (TiO$_2$) nanotubes. These nanotubes, grown on the metallic resonator surfaces, significantly increased the device's active surface area without compromising its fundamental properties. An optimized protocol led to the formation of an ordered array of nanotubes, ≈3 µm thick, ≈3 µm thick, firmly adhered to the Ti6Al4 V surface. This represents a substantial increase in surface area, promoting enhanced sensing capabilities.

In evaluating the practical utility of our resonators, we conducted degradation experiments to monitor the photocatalytic degradation of organic dyes under UV illumination. Remarkably, our nanotube-decorated resonators exhibited high sensitivity, enabling real-time monitoring of dye degradation. The achieved sensitivity enabled the detection of minute frequency variations, with a theoretical sensor resolution below 10 ppb for the first two resonance modes. Moreover, the weak coupling peaks provided insights into the degradation kinetics, offering a comprehensive understanding of the process dynamics. Continuous monitoring of all resonators within the array during degradation experiments proved instrumental in accurately elucidating the degradation kinetics.

In conclusion, our study highlighted the potential of 3D printed metallic resonators, functionalized with TiO$_2$ nanotubes, for high-performance sensing applications. These resonators offer simplicity in fabrication, coupled with enhanced sensitivity and throughput. Through meticulous experimentation and validation, we have demonstrated their efficacy in real-time monitoring of chemical processes, paving the way for their application in environmental monitoring and wastewater treatment.

4. Experimental Section

Ti6Al4 V Sample Preparation: The gas atomized Ti6Al4 V powder was used to fabricate samples with a EOSINT M270 Dual Mode version additive manufacturing machine. A 200 W Yb fiber laser system was used to melt the metallic powders in Ar atmosphere, with an O$_2$ level below 0.1%. Further details about the process parameters and the scanning strategy implemented in this work are already reported in.[30] After the sample printing, excess powder was removed and the component detached from the substrate, a metallic platform needed to give mechanical and thermal support. Detachment from the support occurs following a stress-relieving heat treatment at 680 °C for 2 h in high vacuum (10^{-5} mbar) to reduce thermal stresses that originate during the LPBF process and could otherwise result in sample distortions and dimensional tolerance losses.

The 3D samples fabricated by LPBF approach are composed of a parallelepiped base of 10 mm x 20 mm x1.2 mm (width, length and thickness), with on top a 16×16 pillars matrix of 200 µm diameter and 1.5 mm height.

TiO$_2$ Nanotubes Growth: The Ti6Al4 V specimens produced through LPBF processing served as an initial substrate for growing TiO$_2$ nanotubes. Following a thorough cleaning procedure involving ultrasonication in acetone, rinsing with ethanol, and drying with a stream of nitrogen, the substrates underwent etching in a 1 wt% HF solution to create a fresh metal surface conducive to nanotube nucleation. Anodization occurred at ambient temperature within an electrolyte comprised of ethylene glycol, 0.5 wt% NH$_4$F, and 2.5 vol.% deionized water. This process took place in a two-electrode electrochemical cell supported by Teflon holders, utilizing a platinum foil (250um thick, 99,9 purity, Goodfellow) as the counter electrode. The growth of nanotubes involved a three-step anodization process under continuous stirring, applying a constant voltage of 60 V via a DC power supply (GW Instek SPD-3606). Following anodic oxidation, the samples underwent thermal treatment by annealing in air at 450 °C for 1 h to crystallize TiO$_2$ into the anatase phase. The underlying Ti6Al4 V structure itself served as the bottom electrode for subsequent electrochemical tests.

Characterization: Electron microscope characterization was performed by Field Emission Scanning Electron Microscopy (FESEM, Zeiss Supra 40).

The vibrational analysis of metallic mechanical resonators was performed with a Laser Doppler Vibrometer (LDV MSA-500, Polytec Gmbh). The device was attached to a piezoelectric disk via adhesive tape. The vibrational spectra were recorded by actuating the piezodisk with a sinusoidal chirp signal generated by the LDV system in the desired frequency range and assessing the device response using FFT techniques (Fast Fourier Transform). Measurements were carried out at ambient temperature in a home-made chamber with the possibility to be evacuated by a vacuum system consisting of a membrane and turbomolecular pumps up to a vacuum level of 2×10^{-7} mbar (HiCube80 Eco, Pfeiffer).

The frequency fluctuations of the 3D printed devices are evaluated by means of the Allan deviation measured by analyzing the voltage signal extracted from LDV with a lock-in amplifier (UHFLI, Zurich instruments). The Allan deviation is evaluated in an open-loop configuration by measuring the response of the resonator actuated at a fixed driving frequency (the resonance frequency). The phase of the vibration signal is monitored and then transformed into frequency values from the phase response of the resonator, which is linear close to the resonance frequency. The frequency values are then used to compute the Allan deviation, σ_a in the integration time τ:

$$\sigma_a = \sqrt{\frac{1}{2(N_a - 1)} \sum_{i=2}^{N} \left(\frac{\bar{f}_i - \bar{f}_{i-1}}{f_0} \right)^2}, \tag{5}$$

where $\bar{f}_i$ is the time average of the frequency measurement in the ith time interval of duration τ, N_a is the total number of time intervals, and f_0 is the mean resonance frequency over the duration of the measurement.

Photocatalytic Degradation Analysis: Methylene Blue (MB) (200 µM) solution was prepared starting from 3.6 mM commercial MB solution

(from Sigma). A calibration curve was obtained by considering the characteristic UV absorbance value of MB $\lambda = 610$ nm, obtained for different solutions prepared at prefixed concentration values. The printed resonator arrays was immersed in the MB solution for 20 min to uptake the organic dye to the device surface. Photodegradation experiments were performed by using a UV fiber lamp (HAMAMATSU, LC8). The distance between the device and the source was fixed at 8 cm to ensure 150 mW cm^{-2} of UV light irradiation intensity. After degradation experiments, the device was immersed for 20 min in DI water to remove the remaining dye from the sample and evaluate the percentage of degraded molecule.

Conflict of Interest

The authors declare no conflict of interest.

Data Availability Statement

The data that support the findings of this study are available from the corresponding author upon reasonable request.

[1] J. L. Arlett, E. B. Myers, M. L. Roukes, *Nat. Nanotechnol.* **2011**, *6*, 203.
[2] C. Ricciardi, K. Santoro, S. Stassi, C. Lamberti, M. G. Giuffrida, M. Arlorio, L. Decastelli, *Sens. Actuators, B* **2018**, *254*, 613.
[3] J. Tamayo, P. M. Kosaka, J. J. Ruz, Á. San Paulo, M. Calleja, *Chem. Soc. Rev.* **2013**, *42*, 1287.
[4] J. Moser, A. Eichler, J. Güttinger, M. I. Dykman, A. Bachtold, *Nat. Nanotechnol.* **2014**, *9*, 1007.
[5] C. Chen, S. Rosenblatt, K. I. Bolotin, W. Kalb, P. Kim, I. Kymissis, H. L. Stormer, T. F. Heinz, J. Hone, *Nat. Nanotechnol.* **2009**, *4*, 861.
[6] C. Samanta, S. L. De Bonis, C. B. Møller, R. Tormo-Queralt, W. Yang, C. Urgell, B. Stamenic, B. Thibeault, Y. Jin, D. A. Czaplewski, F. Pistolesi, A. Bachtold, *Nat. Phys.* **2023**, *19*, 1340.
[7] E. Sage, M. Sansa, S. Fostner, M. Defoort, M. Gély, A. K. Naik, R. Morel, L. Duraffourg, M. L. Roukes, T. Alava, G. Jourdan, E. Colinet, C. Masselon, A. Brenac, S. Hentz, *Nat. Commun.* **2018**, *9*, 3283.
[8] A. C. Ceccacci, C.-H. Chen, En-Te Hwu, L. Morelli, S. Bose, F. G. Bosco, S. Schmid, A. Boisen, *Sens. Actuators, B* **2017**, *241*, 1303.
[9] S. Olcum, N. Cermak, S. C. Wasserman, K. S. Christine, H. Atsumi, K. R. Payer, W. Shen, J. Lee, A. M. Belcher, S. N. Bhatia, S. R. Manalis, *Proc Natl Acad Sci U S A* **2014**, *111*, 1310.
[10] I. Ferrante, N. Ciprianetti, S. Stassi, K. Santoro, S. Ferrero, L. Scaltrito, C. Ricciardi, *J. Microelectromech. Syst.* **2017**, *26*, 246.
[11] S. Stassi, G. De Laurentis, D. Chakraborty, K. Bejtka, A. Chiodoni, J. E. Sader, C. Ricciardi, *Nat. Commun.* **2019**, *10*, 3647.
[12] T. Dinh, M. Rais-Zadeh, T. Nguyen, H.-P. Phan, P. Song, R. Deo, D. Dao, N.-T. Nguyen, J. Bell, *Adv. Mater. Technol.* **2024**, *9*, 2300913.
[13] S. Grall, I. Dufour, V. Aubry, H. Debéda, *Smart Mater. Struct.* **2019**, *28*, 105055.
[14] N. Shiraishi, T. Ikehara, D. V. Dao, S. Sugiyama, Y. Ando, *Sens. Actuators, A* **2013**, *202*, 233.
[15] P. Urwyler, H. Schift, J. Gobrecht, O. Häfeli, M. Altana, F. Battiston, B. Müller, *Sens. Actuators, A* **2011**, *172*, 2.
[16] D. Thuau, C. Laval, I. Dufour, P. Poulin, C. Ayela, J. B. Salmon, *Microsyst. Nanoeng.* **2018**, *4*, 15.
[17] S. Stassi, E. Fantino, R. Calmo, A. Chiappone, M. Gillono, D. Scaiola, C. F. Pirri, C. Ricciardi, A. Chiadò, I. Roppolo, *ACS Appl. Mater. Interfaces.* **2017**, *9*, 19193.
[18] I. Roppolo, A. Chiappone, A. Angelini, S. Stassi, F. Frascella, C. F. Pirri, C. Ricciardi, E. Descrovi, *Mater. Horiz.* **2017**, *4*, 396.
[19] N. Alsharif, A. Burkatovsky, C. Lissandrello, K. M. Jones, A. E. White, K. A. Brown, *Small* **2018**, *14*, 1800162.
[20] Y. Yoon, I. Chae, T. Thundat, J. Lee, *Adv. Mater. Technol.* **2019**, *4*, 1800597.
[21] R. Calmo, A. Lovera, S. Stassi, A. Chiadò, D. Scaiola, F. Bosco, C. Ricciardi, *Sens. Actuators, B* **2019**, *283*, 298.
[22] C. Credi, A. Fiorese, M. Tironi, R. Bernasconi, L. Magagnin, M. Levi, S. Turri, *ACS Appl. Mater. Interfaces.* **2016**, *8*, 26332.
[23] S. Stassi, I. Cooperstein, M. Tortello, C. F. Pirri, S. Magdassi, C. Ricciardi, *Nat. Commun.* **2021**, *12*, 6080.
[24] S. Chowdhury, N. Yadaiah, C. Prakash, S. Ramakrishna, S. Dixit, L. R. Gupta, D. Buddhi, *J. Mater. Res. Technol.* **2022**, *20*, 2109.
[25] A. Casu, A. Lamberti, S. Stassi, A. Falqui, *Nanomaterials* **2018**, *8*, 40.
[26] A. Lamberti, N. Garino, K. Bejtka, S. Bianco, S. Stassi, A. Chiodoni, G. Canavese, C. F. Pirri, M. Quaglio, *New J. Chem.* **2014**, *38*, 2024.
[27] A. Lamberti, A. Sacco, S. Bianco, D. Manfredi, F. Cappelluti, S. Hernandez, M. Quaglio, C. F. Pirri, *Phys. Chem. Chem. Phys.* **2013**, *15*, 2596.
[28] A. Lamberti, A. Sacco, S. Bianco, D. Manfredi, M. Armandi, M. Quaglio, E. Tresso, C. F. Pirri, *Sol. Energy* **2013**, *95*, 90.
[29] A. Lamberti, C. F. Pirri, *J. Energy. Storage.* **2016**, *8*, 193.
[30] A. Lamberti, D. Manfredi, F. Calignano, C. F. Pirri, *Mater. Today. Commun.* **2018**, *15*, 165.
[31] E. Gil-Santos, D. Ramos, A. Jana, M. Calleja, A. Raman, J. Tamayo, *Nano Lett.* **2009**, *9*, 4122.
[32] C. Zhao, M. H. Montaseri, G. S. Wood, S. H. Pu, A. A. Seshia, M. Kraft, *Sens. Actuators, A: Phys.* **2016**, *249*, 93.
[33] S. Stassi, A. Chiadò, G. Calafiore, G. Palmara, S. Cabrini, C. Ricciardi, *Sci. Rep.* **2017**, *7*, 1065.
[34] S. Stassi, V. Cauda, S. Fiorilli, C. Ricciardi, *J. Mater. Chem. C* **2015**, *3*, 12507.
[35] S. Stassi, A. Chiadò, V. Cauda, G. Palmara, G. Canavese, M. Laurenti, C. Ricciardi, *Anal. Bioanal. Chem.* **2017**, *409*, 2615.
[36] I. Khan, I. Saeed, I. Zekker, B. Zhang, A. H. Hendi, A. Ahmad, S. Ahmad, N. Zada, H. Ahmad, L. A. Shah, T. Shah, I. Khan, *Water* **2022**, *14*, 242.
[37] J. Yao, C. Wang, *Int. J. Photoenergy.* **2010**, *2010*, 643182.
[38] T. S. Natarajan, K. Natarajan, H. C. Bajaj, R. J. Tayade, *Ind. Eng. Chem. Res.* **2011**, *50*, 7753.
[39] R. S. Dariani, A. Esmaeili, A. Mortezaali, S. Dehghanpour, *Optik* **2016**, *127*, 7143.

**ADVANCED
SCIENCE NEWS**

www.advancedsciencenews.com

**ADVANCED
MATERIALS
TECHNOLOGIES**

www.advmattechnol.de

[40] J. Joo, J. Shim, H. Seo, N. Jung, U. Wiesner, J. Lee, S. Jeon, *Anal. Chem.* **2010**, *82*, 3032.

[41] M. Laurenti, N. Garino, G. Canavese, S. Hernandéz, V. Cauda, *ACS Appl. Mater. Interfaces.* **2020**, *12*, 25798.

[42] M. Laurenti, M. Fontana, S. Stassi, A. Sacco, A. Scalia, S. Bianco, C.

F. Pirri, A. Lamberti, *Adv. Mater. Interfaces.* **2023**, *10*, 2300485.

[43] M. C. Paganini, A. Giorgini, N. P. F. Gonçalves, C. Gionco, A. Bianco Prevot, P. Calza, *Catal. Today* **2019**, *328*, 230.

[44] F. Mushtaq, X. Chen, M. Hoop, H. Torlakcik, E. Pellicer, J. Sort, C. Gattinoni, B. J. Nelson, S. Pané, *iScience* **2018**, *4*, 236.

2401142 (9 of 9)